ADVANCED ELECTRONIC MATERIALS Open Access
www.advelectronicmat.de

Toward High-Performance Electrochemical Energy Storage Systems: A Case Study on Predicting Electrochemical Properties and Inverse Material Design of MXene-Based Electrode Materials with Automated Machine Learning (AutoML)

*Berna Alemdag, Görkem Saygili, Matthias Franzreb, and Gözde Kabay**

This study highlights the potential of Automated Machine Learning (AutoML) to improve and accelerate the optimization and synthesis processes and facilitate the discovery of materials. Using a Density Functional Theory (DFT)-simulated dataset of monolayer MXene-based electrodes, AutoML assesses 20 regression models to predict key electrochemical and structural properties, including intercalation voltage, theoretical capacity, and lattice parameters. The CatBoost regressor achieves R^2 values of 0.81 for intercalation voltage, 0.995 for theoretical capacity as well as 0.807 and 0.997 for intercalated and non-intercalated in-plane lattice constants, respectively. Feature importance analyses reveal essential structure-property relationships, improving model interpretability. AutoML's classification module also bolsters inverse material design, effectively identifying promising compositions, such as Mg^{2+}-intercalated and oxygen-terminated ScC_2 MXenes, for high-capacity and high-voltage energy storage applications. This approach diminishes reliance on computational expertise by automating model selection, hyperparameter tuning, and performance evaluation. While MXene-based electrodes serve as a demonstrative system, the methodology and workflow can extend to other material systems, including perovskites and conductive polymers. Future efforts should prioritize integrating AutoML with real-time experimental feedback and hybrid simulation frameworks to create adaptive systems. These systems can iteratively refine predictions and optimize trade-offs among critical metrics like capacity, stability, and charge/discharge rates, driving advancements in energy storage and other material applications.

1. Introduction

Developing sustainable energy technologies is one of the top global priorities due to the depletion of fossil fuels, the rising energy crisis, and the environmental challenges linked to their ongoing use. These highlight the increasing demand to explore advanced materials that enhance the efficiency, durability, capacity, and performance of battery-based electrochemical energy storage (EES) technologies, particularly those that empower electric vehicles, off-grid electricity, and stationary systems.[1–3]

For instance, since their discovery in 2011, MXenes[4]—a family of 2D transition metal carbides and carbonitrides—and their various hybrids have received significant attention in developing electrode materials for batteries, mainly because of their hydrophilicity, tailorable structure, ability to host multiple intercalating ions (e.g., Li^+, Na^+, K^+, Mg^{2+}, and Al^{3+}) and high electrical conductivity ($\approx 2 \times 10^5$ S m^{-1}).[5–7] Also, their adjustable interlayer spacing (from 0.977 nm to ≈3.2 nm) results in faster

The ORCID identification number(s) for the author(s) of this article can be found under https://doi.org/10.1002/aelm.202400818

[Correction added on February 27, 2025, after first Online publication: Affiliation for second author was updated in this version.]

DOI: 10.1002/aelm.202400818

B. Alemdag, M. Franzreb, G. Kabay
Karlsruhe Institute of Technology (KIT)
Department for Bioengineering and Biosystems
Institute of Functional Interfaces (IFG)
76344 Eggenstein-Leopoldshafen, Germany
E-mail: gozde.kabay@kit.edu

G. Saygili
Department of Cognitive Science and Artificial Intelligence
Tilburg University
Tilburg School of Humanities and Digital Sciences (TSHD)
Tilburg 5037 AB, The Netherlands

charge/discharge rates and higher capacity than conventional 2-D materials.[8] 2D MXenes are represented by the general formula of $M_{n+1}X_nT_x$ (n, x = 1, 2, 3). Here, M denotes the early transition metal (e.g., Ti, Nb, Mo), X represents carbon or nitrogen, and T_x stands for the surface functional groups (e.g., —H, —O, —OH, —F) bound to the outer M layers, highlighting their complex yet versatile structural composition.[6,9–11] Nonetheless, this structural complexity leads to performance variations, underscoring the need to explore the connection between physicochemical structure (such as composition, surface chemistry, lateral size, and thickness) and electrochemical properties, including capacity, intercalation voltage, and energy density.

The current approach to studying the structure-property relationship of active electrode materials (forming cathodes and/or anodes) involves experimental and/or computational methods.[12] Experimental techniques, such as charge and discharge cycling, cyclic voltammetry, and electrochemical impedance spectroscopy, provide direct empirical insights in a broad time frame. However, they are often labor- and resource-intensive, time-consuming, and require specialized methods, equipment, and expertise to perform analyses. Yet, they only allow researchers to comprehensively span some potential material configurations.[12] On the other hand, computational approaches such as DFT,[13] molecular dynamics (MD), and Monte Carlo simulations enable the modeling of atomic-scale interactions and the prediction of electrode material properties before synthesis.[12,14] Although they offer the advantage of reducing the number of physical experiments required, i) they still demand substantial computational resources and users with advanced theoretical knowledge to perform simulations, ii) they are highly dependent on the accuracy of theoretical models, and iii) their ability to effectively explore large or complex material design spaces is limited. While combining experimental and computational techniques helps to address the inherent limitations of each, utilizing these methods in tandem to investigate new material configurations remains challenging, especially when multiple material attributes, including composition, surface chemistry, and structure, are assessed simultaneously.[12,14–16] These challenges emphasize the need for more advanced tools and algorithms that analyze the complex relationships between large datasets and predict material properties to streamline the development of high-performance EES systems.

To address these challenges, machine learning (ML) has emerged as a potent tool in materials science because it analyzes substantial datasets and uncovers complex structure-property relationships.[17–21] This data-driven approach significantly reduces reliance on experimental procedures and computer-assisted simulations, leading to faster and more efficient material design and development. However, using traditional ML techniques requires advanced programming skills, complex algorithm creation, and extensive data science knowledge, which are obstacles that hinder its broader use in materials research among those without coding skills.

In response to these limitations,AutoML offers a solution that simplifies the conventional ML workflow while preserving the high predictive accuracy of traditional ML algorithms.[22–24] So far, several AutoML frameworks, namely AutoWeka, AutoSKlearn, TPOT, Recipe, PyCaret, and SmartML, have been utilized to fill the gap of human expertise by automating the process of building ML pipelines to boost productivity.[23–25] Among these frameworks, PyCaret, an open-source ML library in Python, is gathering significant attention due to offering a low-code solution and automating critical steps like data pre-processing, model selection, hyperparameter tuning, and cross-validation.[26] Also, it enables rapid experimentation and simultaneous performance comparison with multiple regression and classification models, which is particularly useful for novel materials design and optimization.

This study demonstrates the first application of AutoML utilizing PyCaret to predict the key electrochemical and structural properties—intercalation voltage [V], theoretical capacity [mAh g^{-1}], and in-plane lattice constants [Å] (intercalated and non-intercalated)—of monolayer MXene-based electrode materials. First, we thoroughly analyzed the performance of 20 regressors using PyCaret's AutoML framework to establish structure-property relationships. Our findings demonstrated AutoML's capability to predict the selected target features while dramatically reducing the time (t < 1 s) and effort associated with feature engineering, model development, training, and performance evaluation. Additionally, with PyCaret's classifier module, we reversed the predictions to discover the molecular formulas of various MXenes, using electrochemical properties as inputs. While MXene-based electrode materials are demonstrated as an illustrative case study, AutoML's broader applicability encompasses other materials, like graphene or perovskites. Overall, this study aims to enable materials scientists to integrate AutoML into their experimental workflows, thereby speeding up the discovery and optimization of high-performance materials for energy storage and other uses.

2. Results and Discussion

2.1. AutoML Model Training and Performance Evaluation by PyCaret

In this study, we performed PyCaret's AutoML framework to predict the electrochemical properties of monolayer MXene-based electrode materials, focusing on intercalation voltage, theoretical capacity, and in-plane lattice parameters (for intercalated and non-intercalated cases). AutoML facilitated the automation of various conventional ML tasks, including feature engineering, regression model selection, hyperparameter tuning, model performance evaluation, and feature importance ranking, allowing the comprehensive comparison of different algorithms without extensive manual manipulation.[27]

The DFT dataset used in this study contains calculations for 360 different monolayer MXene derivatives, represented by the formula $M_{n+1}X_nT_x$. The formulation varies according to the type of transition metal (M = Sc, Ti, V, Cr, Zr, Nb, Mo, Hf, and Ta), which leads to nitride (X = N) or carbide (X = C) derivatives. These derivatives may be either functionalized with functional groups (T = —H, —O, —OH, —F) or non-functionalized (NULL) and can be intercalated with cationic ions (Z = Li^+, Na+, K+, Mg^{2+}) or non-intercalated.[28]

Figure 1 shows the workflow utilized in this study. First, the one-hot-encoded DFT-derived dataset[20,28] was fed into the AutoML pipeline and split into training/test sets at an 85/15% ratio

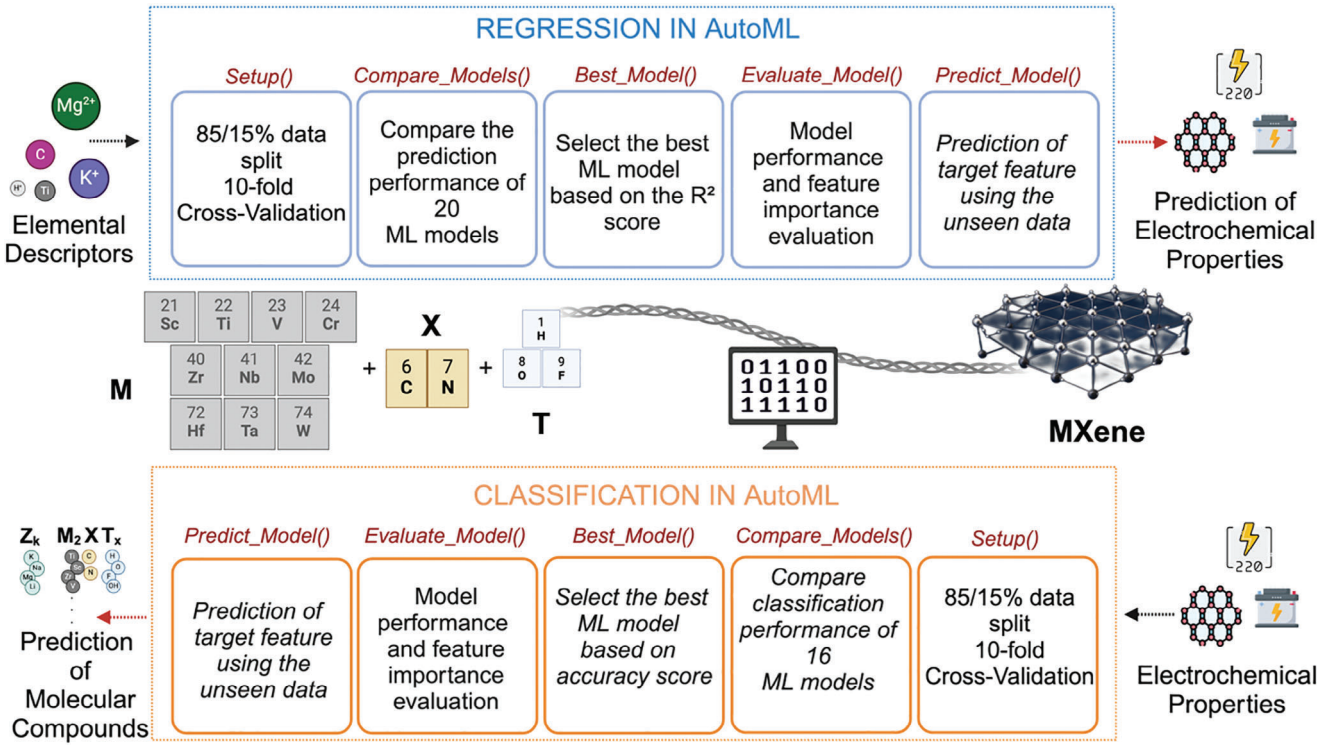

Figure 1. AutoML workflow for predicting electrochemical and structural properties of monolayer MXene-based electrode materials and inverse prediction of molecular formula, both achieved using the PyCaret framework.

to ensure sufficient data for training while retaining enough data to test the model's generalization capabilities. For each model, 10-fold cross-validation (CV) was applied during the *create_model()* step to ensure robust performance estimates. The dataset was divided into ten subsets (nine splits for training and a single split for testing for each fold) to reduce overfitting and provide reliable results. Yet, the relatively small dataset (n = 364) we used in this study possesses the risk of overfitting and creating bias. A Bayesian leave-one-out (LOO) CV was performed to mitigate these risks and fine-tune the performance of the best-performing model. This technique is a form of k-fold cross-validation where the number of folds, k, equals the total number of data points in the dataset. It iteratively removes one observation from the dataset, trains the model on the remaining data, and tests it on the held-out observation for model evaluation and selection (Table S2, Supporting Information).[29]

The prediction accuracy of the 20 selected regression algorithms was ranked using the R^2 (coefficient of determination) metric through the *compare_models()* function to identify and rank which models most effectively captured the variation in each target feature's prediction. Although R^2 is a valuable metric for explaining the variance between the model predictions and the actual data, R^2 alone can be insufficient, especially in complex materials science applications where prediction errors are critical. Therefore, we also consider other performance metrics, root mean square error (*RMSE*), mean absolute error (*MAE*), and mean absolute percentage error (*MAPE*), for model performance comparison across different target features (Table S1, Supporting Information). Hyperparameter tuning in random grid search mode was prompted by the *tune_model()* function to optimize the best-performing models further. This step was crucial in ensuring the models were high-performing and robust across different hyperparameter settings, reducing the risk of overfitting and improving model stability. Then, the *evaluate_model()* function was used to evaluate performance insights for each target variable: intercalation voltage, theoretical capacity, and in-plane lattice constants.

2.1.1. Voltage

Voltage, generally measured in Volts or [*V*], refers to the electrochemical potential difference between the battery's terminals or two electrodes—typically a cathode (positive terminal) and an anode (negative terminal).[30] It often reflects the total energy or power output that a battery can deliver to an external circuit, which varies based on how many electrochemical cells are used to construct the battery and how they are positioned. On the other hand, the cell voltage refers to the voltage of a single electrochemical cell constituting a battery, allowing electric charges to move through an external circuit while discharging. It is typically influenced by electrolyte type, electrode material, and structural properties.[2] For example, Li-ion batteries have higher cell potential (≈2.5–4.2 V per cell) than nickel-cadmium ones (Ni-Cd ≈1.2 V per cell) because Li-ion has a higher electrochemical potential.[31] Another important voltage parameter is intercalation voltage, which reflects the material's capacity to host intercalating ions (e.g., Li^+, Na^+, Mg^{2+}), a critical factor in battery

Table 1. A list of performance metrics, including R^2, MAE, RMSE, MAPE, and TT, was obtained by evaluating the three top-performing regression algorithms for predicting intercalation voltage, theoretical capacity, and in-plane lattice constant (both intercalated and non-intercalated). All regression models were trained and tested using an 85/15% train/test split.

Target feature[unit]	Regression model	R^2	MAE	RMSE	MAPE	TT[s]
Intercalation Voltage[V]	CatBoost	0.810	0.164	0.264	0.816	0.421
	GBR	0.758	0.197	0.295	0.976	0.165
	XGBoost	0.751	0.177	0.297	1.086	0.113
Theoretical capacity [mAh g^{-1}]	CatBoost	0.995	4.729	8.933	0.016	0.796
	XGBoost	0.993	5.532	11.239	0.017	0.083
	RF	0.993	8.247	11.557	0.029	0.453
In-plane lattice constant (non-intercalated) [Å]	CatBoost	0.997	0.007	0.009	0.002	0.442
	XGBoost	0.990	0.009	0.014	0.003	0.129
	DT	0.990	0.001	0.006	0.004	0.028
In-plane lattice Constant (intercalated) [Å]	CatBoost	0.807	0.040	0.062	0.013	0.452
	LightGBM	0.803	0.046	0.063	0.015	0.467
	RF	0.786	0.043	0.066	0.014	0.229

*Acronyms: Coefficient of Determination, R^2; Mean Absolute Error, MAE; Root Mean Squared Error, RMSE; Mean Absolute Percentage Error, MAPE; TT, Training Time; Categorical Boosting, CatBoost; Gradient Boosting Regressor, GBR; eXtreme Gradient Boosting, XGBoost; Random Forest, RF; Decision Tree: DT; Light Gradient Boosting Machine, LightGBM.

development that influences energy density, charge/discharge rates, and overall battery performance.[30] Given its significance in determining battery efficiency, we initially evaluated various regression algorithms to predict this parameter, providing a more precise and efficient approach for optimizing MXene-based battery systems.

According to **Table 1**, the CatBoost Regressor (CatBoost) emerged as the most effective model for predicting the intercalation voltage, outperforming other models ($R^2 = 0.810$, $MAE = 0.164$, $RMSE = 0.264$, and $MAPE = 0.816$). The R^2 signifies that the model explained 81% of the variance in the data; despite having a slightly longer model training time (TT) of 0.421 s, the prediction performance justified this trade-off. The Gradient Boosting Regressor (GBR) performed reasonably well, with an $R^2 = 0.758$. However, the prediction errors ($MAE = 0.197$, $RMSE = 0.295$, and $MAPE = 0.976$) were higher than those of CatBoost. While GBR's TT was shorter than CatBoost's (0.172 vs 0.421 s), its lower prediction performance made it less appropriate. On the other hand, the eXtreme Gradient Boosting (XGBoost) algorithm yielded the lowest R^2 among others with an R^2 of 0.75 but the shortest TT of 0.113 s. Yet, the high errors obtained while performing the XGBoost ($MAE = 0.177$, $RMSE = 0.297$, and $MAPE = 1.086$) model made it a less preferable option overall.

2.1.2. Capacity

Capacity, along with intercalation voltage, is a crucial parameter determining battery performance. It directly impacts how long a battery can operate per cycle and informs about the overall energy efficiency of an EES system. Material composition, temperature, charge-discharge rate, and aging influence capacity, making it a key investigation focus in battery technologies.[7,32,33] Theoretical capacity refers to the maximum amount of electrical charge ampere-hours or milliampere-hours [Ah or mAh] stored or delivered per gram [g] of the active electrode material within a battery. It is represented as [mAh g^{-1}] and is typically determined by the chemical composition and structure of the electrode material, as well as the number of electrons involved in redox reactions. These redox reactions, the primary mechanism for storing and releasing electrical energy in batteries, involve the transfer of ions (such as Li^+ or other intercalating species) between the anode and cathode electrodes. It is important to note that it is a theoretical value calculated by assuming ideal conditions, leading to perfect utilization of the active electrode material so that complete reduction or oxidation occurs. However, in practice, electrode materials rarely reach their theoretical capacity due to side reactions, incomplete active material, and structural degradation.[7,32,34,35] Theoretical capacity is a critical factor while designing high-performance batteries. Therefore, it is chosen as the second target feature for prediction in AutoML.

The performance analysis results suggest that CatBoost indicated the highest performance in predicting the theoretical capacity of MXenes. *The* R^2 value of 0.995 indicates that the model explained 99.54% of the variance. Also, CatBoost introduced minimal errors in its predictions ($MAE = 4.729$, $RMSE = 8.994$, and $MAPE = 0.016$). Even though its TT was not the fastest (0.796 s), the extraordinary model fitting performance compensated for this. The XGBoost regressor also performed well with theoretical capacity prediction, indicated by the R^2 of 0.993, which correlated to 99.34% variance prediction, only slightly less sensitive than CatBoost's. Despite having higher error rates ($MAE = 5.532$, $RMSE = 11.239$, and $MAPE = 0.017$), XGBoost's rapid training capability (0.083 s) makes it a viable option in terms of speed and a promising alternative to CatBoost when working with larger datasets. The third best-performing model was selected as the Random Forest (RF), mainly because it is still a rapid algorithm for training ($TT = 0.453$ s), and given the R^2 score of 0.993, its prediction capability of 99.29% variance is sufficient. However,

higher prediction errors (MAE = 8.247, $RMSE$ = 11.557, and $MAPE$ = 0.029) obtained than those of CatBoost and RF indicate the training speed and R^2 score may not compensate for its disadvantages.

2.1.3. In-Plane Lattice Constants

A crystal structure is defined by a lattice constant (also known as lattice parameter), which refers to the length of the edges of the unit cell represented with a length unit of Ångström or [Å]. For 2D materials like MXene, there are two essential lattice constants: in-plane and out-of-plane. The in-plane lattice constant measures the periodic spacing between atoms in the same plane (in the x-y plane), while the out-of-plane lattice constant refers to the spacing between adjacent layers (along the z-axis). Intercalating with donor and acceptor ions typically causes the expansion and contraction of the electrode material's lattice, directly affecting the electrode's electronic, mechanical, and electrochemical properties. Correspondingly, the regression algorithms' prediction performances for in-plane lattice constant in the presence and absence of intercalating ions were evaluated.

The analysis results given in Table 1 reveal that CatBoost exhibited superior performance in predicting the in-plane lattice constant for non-intercalated MXene-based electrodes. The R^2 value of 0.997 suggests that the model explained 99.7% of the variance in the in-plane lattice constant. It also demonstrated minimal prediction errors, with MAE = 0.007, $RMSE$ = 0.009, and $MAPE$ = 0.022. Despite a TT of 0.442 s, the model's predictive power justifies the modest increase in training time, making CatBoost a suitable choice when prioritizing precision over speed in lattice constant predictions. The second best-performing model, XGBoost, also performed well, with an R^2 of 0.990, explaining 99.0% of the variance, slightly less than CatBoost's. It showcased slightly better absolute error rates, achieving MAE = 0.009, although $RMSE$ = 0.014 and $MAPE$ = 0.003 were marginally higher. Notably, XGBoost's TT of 0.129 s is about three times faster than CatBoost. It is a suitable choice when computational efficiency is crucial, particularly for larger datasets or real-time predictions where rapid retraining is critical. Ultimately, the performance of the third best-performing model, Decision Tree (DT), is evaluated. While competitive regarding R^2 (0.990), it also exhibited the best error metrics (MAE = 0.001, $RMSE$ = 0.006, and $MAPE$ = 0.004) at the shortest TT of 0.028 s. However, these minimal absolute errors may be caused by the model's tendency to overfit, mainly when generalizing to larger or more complex datasets. Considering its lower R^2 and the possibility of overfitting, CatBoost is the best model for predicting the in-plane lattice constant for non-intercalated MXene-based electrodes.

For the intercalated electrode configuration, CatBoost again demonstrated the highest prediction performance (80.7%), with an R^2 of 0.807. The prediction errors were minimal, with MAE = 0.040, $RMSE$ = 0.062, and $MAPE$ = 0.013, making it a highly accurate choice for this task. Despite its longer training time of 0.452 s, CatBoost's R^2 value positions it as a strong candidate for lattice constant predictions, mainly when variance prediction is the primary concern. LightGBM also performed well for the intercalated case, with an R^2 of 0.803, explaining 80.3% of the variance. The error rates were slightly higher than CatBoost, with MAE = 0.046, $RMSE$ = 0.063, and $MAPE$ = 0.015, but these differences are marginal. Its TT of 0.467 s is comparable to CatBoost, making it a competitive alternative for applications accommodating slightly higher error rates. Random Forest (RF), with an R^2 of 0.786, was less accurate in explaining the variance for the intercalated case. However, its MAE of 0.043 and $RMSE$ of 0.066 were still competitive, and a $MAPE$ = 0.014 suggests a negligible percentage error. The RF model was significantly faster in training, with a TT of 0.229 s, making it a robust option when computational speed is a priority.

Moreover, CatBoost consistently delivers the highest predictive power across in-plane lattice parameter prediction both for intercalated and non-intercalated cases. Still, XGBoost and RF offer competitive alternatives depending on the trade-off between speed and precision. In contrast, the DT model excels in error minimization for non-intercalated configuration but may overfit, while LightGBM provides a balanced alternative for intercalated lattice constant predictions. For a detailed comparative evaluation of the performance of the top ten algorithms regarding each target feature prediction, please refer to **Figure 2**.

2.2. Feature Importance Analysis

To develop high-performance batteries, it is essential to carefully determine the structural features of the electrode material within a complex design space that includes multiple variables, such as the elemental composition of the electrode material, functional groups, and intercalating ions. This complexity complicates identifying optimal material combinations solely through experimental methods and/or computer-assisted simulations, particularly given the time and resource constraints.[3,15,18,34,36]

Feature importance analysis provided by ML simplifies the selection process of elemental descriptors by assessing the relative significance of each input parameter for predicting target features. This method allows researchers to navigate the complex design space efficiently. When performed in AutoML, as demonstrated in this study using the PyCaret framework, it delivers an automated solution to rapidly and automatically identify the most critical features that influence the prediction of target variables. By incorporating this automated tool into their experimental workflow, researchers can save time, effort, and resources while optimizing electrode material features to facilitate high-performance EES development. After determining the best-performing ML model to be CatBoost for each target feature's prediction, PyCaret's feature importance function is prompted to evaluate the significance of different elemental descriptors on the CatBoost algorithm's predictive power of the target features—intercalation voltage, theoretical capacity, and in-plane lattice constant (intercalated vs non-intercalated). Lastly, SHAP (SHapley Additive exPlanations) analyses were performed by CatBoost to assess each input parameter's contribution (high or low) to target feature prediction. The respective SHAP plots are shown in Figure S2 (Supporting Information).

The feature importance plot in **Figure 3a** highlights that the K^+ intercalating ions, —O, and —OH functional groups significantly contribute to CatBoost's intercalation voltage prediction performance. K^+ has the highest feature importance, as these ions substantially influence the potential difference due to intercalation. Due to its large effective ionic radius (1.81 Å),

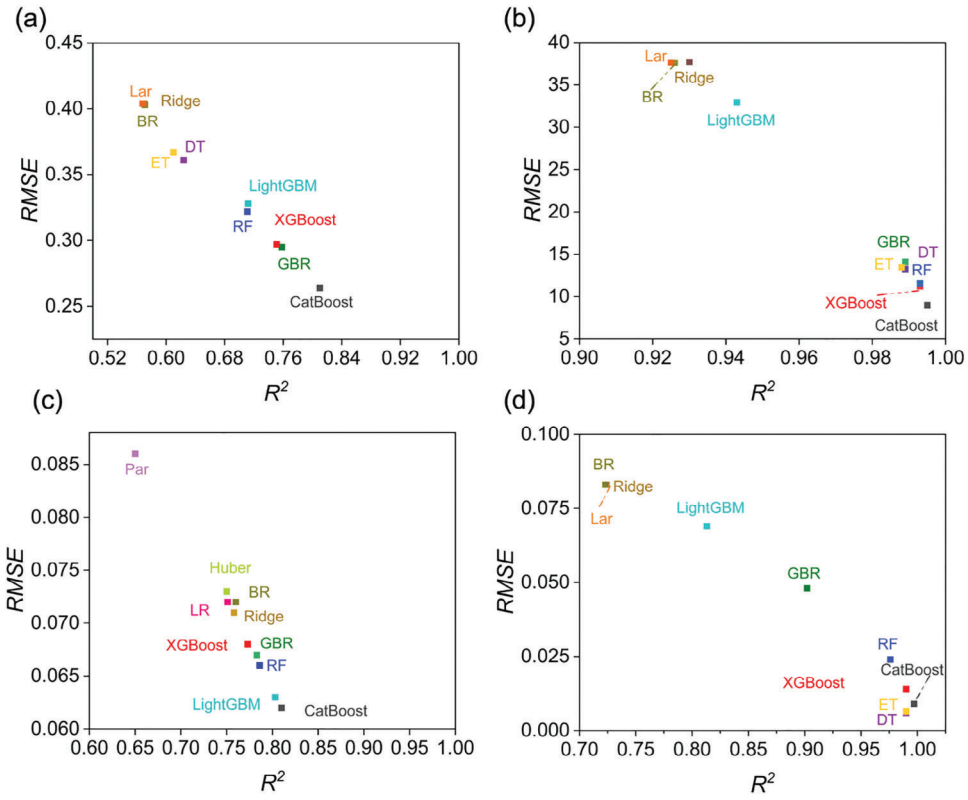

Figure 2. A comparative evaluation of performance metrics for the top 10 best-performing regression models regarding a) intercalation voltage, b) theoretical capacity, c) in-plane lattice constant for intercalated, and d) non-intercalated monolayer MXene-based electrode materials.

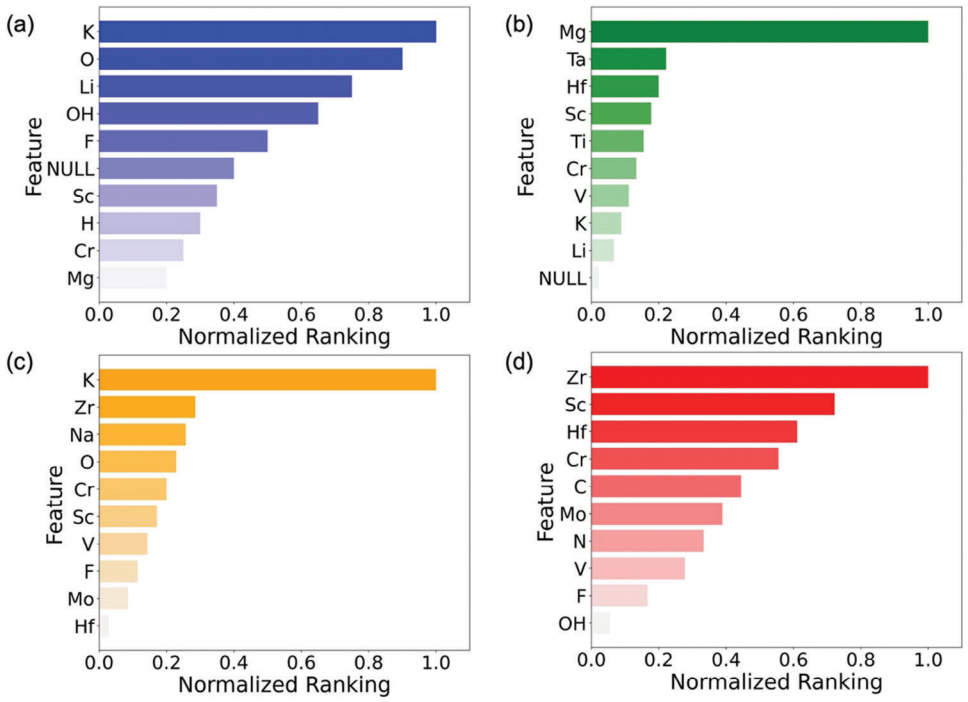

Figure 3. The normalized ranking of elemental descriptors' importance for predicting target features using the CatBoost ML algorithm. The target features include a) intercalation voltage, b) induced charge, c) in-plane lattice constant for intercalated MXenes, and d) non-intercalated monolayer MXene-based electrode materials.

K^+ may induce significant structural changes in the material lattice, directly impacting the electrochemical potential of the electrode.[37] This observation aligns with SHAP analyses (Figure S2a, Supporting Information) and earlier findings, which noted that larger intercalating ions, such as K^+, improve structural stability and intercalation voltage performance in MXene-based EES systems.[38] The influences of —O and —OH surface terminations are also notable in voltage prediction, as both functional groups affect the electrochemical behavior of the produced batteries, likely by providing active sites for redox reactions or altering their redox potential.[20,39] In summary, the larger ionic size of K^+ likely leads to considerable alterations in the electrochemical double layer, whereas —O and —OH surface terminations play a crucial role in modifying the electronic structure of $M_{n+1}X_nT_x$, further influencing intercalation voltage. Li^+ intercalation and —F surface termination also display moderate importance in voltage. Li^+ is the smallest intercalating ion with a 0.60 Å ionic radius that can quickly move within the T_3C_2 layers during charge/discharge cycles, altering the intercalation voltage and contributing positively to voltage stability. Interestingly, the NULL feature, representing a bare electrode without surface terminations, shows moderate importance in intercalation voltage, confirming previous findings.[40] On the other hand, molybdenum (Mo), hydrogen (H), scandium (Sc), and magnesium (Mg) are of lower importance, suggesting that while they do influence voltage output, their effects are less significant compared to others. Despite its critical function in charge storage, the lesser role of Mg-ions implies that its impact on intercalation voltage prediction is more limited compared to the structural and surface changes induced by K^+ and oxygen-based terminations. K^+ ions have the highest SHAP values, significantly impacting the intercalation voltage prediction.

The feature importance analysis for theoretical capacity prediction highlights the dominance of Mg^{2+} intercalating ion followed by tantalum (Ta) and hafnium (Hf) transition metals (Figure 3b). Mg^{2+}, as a divalent ion, plays a critical role in the gravimetric capacity by storing more charge per unit of mass compared to monovalent ions like Li^+, K^+, and Na^+.[6,7] This higher charge density makes Mg^{2+} ions an ideal candidate for maximizing charge storage, leading to high-capacity energy storage, whether used for intercalation of monolayer or multilayered MXene-based electrode materials.[7] Transition metals, Ta and Hf, are also crucial for capacity prediction, as they contribute to the structural stability of the MXene-based electrodes. This stability allows for greater intercalation and ion deintercalation while eliminating the risk of structural degradation. Such stability helps maintain the integrity of MXenes during repeated ion cycling, which is vital for achieving high-capacity battery development. While Sc, chromium (Cr), titanium (Ti), and vanadium (V) show moderate importance, their contributions likely relate to their ability to support the robustness of the MXene-based electrode structures by facilitating ion storage. The NULL feature further highlights that even bare $M_{n+1}X_n$ can contribute to capacity, though minor. SHAP plots also confirm that Mg^{2+} ions have the highest positive impact on the theoretical capacity, followed by Ta and Hf. Conversely, elements such as Sc, Ti, and Cr have a moderate influence, evidenced by their lower SHAP values (Figure S2b, Supporting Information). This underscores the importance of intercalating multivalent ions and transition elements for high-capacity and robust MXene-based batteries that can empower high-performance EES systems.

The intrinsic properties of the core transition metals and intercalating ions predominantly determine the in-plane lattice parameter. Particularly for monolayer materials, the in-plane lattice parameter is a crucial determinant of the material's structural and electrochemical properties. Upon monolayer MXenes intercalation, alterations in the in-plane lattice parameters occur as ions expand or compress the atomic spacing.[41] For instance, K^+ ions cause significant lattice expansion, facilitating ions' diffusion and transport within the material. Na^+ ions trigger moderate lattice expansion, balancing improved ion transport with structural stability. Mg^{2+} ions cause less lattice expansion yet enhance energy density due to their capacity to store more charge per unit of the material.

The feature importance plot (Figure 3c) for the ion intercalated monolayer MXene suggests that K^+ is the primary feature affecting the in-plane lattice parameter among other elemental descriptors. Following K^+, the d-orbitals in transition metals like Zr, Sc, and Hf allow for strong bonding interactions within the MXene layers, contributing to mechanical stability and enhanced ion accommodation during intercalation. This ensures the electrode material can accommodate intercalating ions without significant collapse or lattice degradation, ensuring robustness during charge/discharge cycles and contributing to long-term battery performance. The SHAP plots in Figure S2c (Supporting Information) further demonstrate that elevated K^+ levels greatly enhance the lattice, while the SHAP values for Zr and Na point to a lesser expansion effect when compared to K^+. Regarding functional groups, —O interacts with intercalating cations, stabilizing the lattice and enhancing the MXenes's electronic structure. —F and —OH functional groups primarily affect the surface reactivity and electrochemical behavior of the MXene-based electrode by modifying the surface chemistry. However, their direct influence on the in-plane lattice parameter is minimal compared to the intercalating ions.

In the non-intercalated scenario (Figure 3d), where no ions are inserted into the MXene structure ($M_{n+1}X_nT_x$), the in-plane lattice parameter is primarily influenced by the atomic composition. Zr, Sc, and Hf are the key transition metals that dominate the atomic arrangement in monolayer MXenes. Their large atomic radii dictate the spacing between atoms within the 2D monolayer and influence the lattice constant. Zr plays a significant role in maintaining the mechanical strength of the lattice by ensuring that the atomic spacing remains consistent, contributing to the overall robustness of the electrode material.[42] Similarly, Sc and Hf, which share similar atomic radii to that of Zr, reinforce the structural integrity of the MXene by balancing atomic spacing and contributing to its mechanical and thermal stability. SHAP plots reveal that Zr has the most significant impact in the non-intercalated scenario. Higher Zr levels increase the in-plane lattice parameter, whereas lower levels decrease it. Furthermore, Sc and Hf also play a crucial role; increasing their content results in larger in-plane lattice spacing, evident from their positive SHAP values (Figure S2d, Supporting Information). Cr and Mo show moderate importance in maintaining structural stability, mainly by influencing the bonding between metal layers and the crystal structure. Surface terminations like —F and —OH are more significant in influencing out-of-plane parameters or

Table 2. Classification performance metrics that are calculated for the best-performing Gradient Boosting Classifier (GBC) model for each target feature (or category).

Target feature	Classification model	Accuracy	AUC	Precision	F1 score	*TT* [s]
M	GBC	0.823	0.99	0.855	0.816	1.071
X		0.913	0.98	0.902	0.913	0.150
T		0.749	0.94	0.769	0.744	0.568
Z		0.854	0.96	0.860	0.845	0.755

electrochemical reactions than directly impacting the in-plane lattice parameter, as their primary influence is on surface chemistry and electrochemical reactivity rather than the core structure.

2.3. Inverse Prediction of Molecular Composition

Inverse prediction of material molecular composition plays a crucial role in designing and discovering new materials with the desired functionality. We utilized PyCaret's classification module to achieve this, and the molecular formulas representing prospective MXene structures with the assigned electrochemical properties were generated. First, the MXene molecular formula components are grouped into four categories (M: transition metal, X: core atom, T: functional group, Z: intercalating ions), which merge the 20-dimensional dataset utilized in the forward prediction into a 4D vector for inverse prediction. Then, elemental descriptors (e.g., Nb, —O, Mg^{2+}, NULL) representing each category are label-encoded as follows:

$$\mathrm{M}: \mathrm{Sc} \rightarrow 0, \mathrm{i} \rightarrow 1, \mathrm{V} \rightarrow 2, \mathrm{Cr} \rightarrow 3, \mathrm{Zr} \rightarrow 4, \mathrm{Nb} \rightarrow 5, \mathrm{Mo} \rightarrow 6, \mathrm{Hf} \rightarrow 7, \mathrm{Ta} \rightarrow 8 \quad (1)$$

$$\mathrm{X}: \mathrm{C} \rightarrow 0, \mathrm{N} \rightarrow 1 \quad (2)$$

$$\mathrm{T}: \mathrm{NULL} \rightarrow 0, \mathrm{H} \rightarrow 1, \mathrm{O} \rightarrow 2, \mathrm{OH} \rightarrow 3, \mathrm{F} \rightarrow 4 \quad (3)$$

$$\mathrm{Z}: \mathrm{Li}^{+} \rightarrow 0, \mathrm{Na}^{+} \rightarrow 1, \mathrm{K}^{+} \rightarrow 2, \mathrm{Mg}^{2+} \rightarrow 3 \quad (4)$$

the classification algorithm's training and performance testing were conducted. The classification performance of 16 classifiers for each category is determined by calculating performance metrics, including accuracy, area under the curve (AUC), recall, precision, F1-score, and *TT* (**Table 2**). All classifiers are ranked based on their AUC value, and the best-performing one in each category is used to evaluate the receiver operating characteristic (ROC) curve (Figure S3, Supporting Information), confusion matrix (Figure S4, Supporting Information), and the global feature of importance plots (Figure S5, Supporting Information), all of which are given in *Supporting Information* document.

The gradient boosting classifier (GBC) performed well across all categories, achieving 82.35% accuracy for M prediction and indicating robust classification of transition metals. It excelled with 91.25% accuracy in differentiating C and N core atoms but struggled with T predictions at 74.90%, reflecting the complexity of categorizing functional groups. GBC performed well for Z with 85.43% accuracy and identified intercalating ions successfully.

The AUC metric within the ROC curve assesses a model's capacity to distinguish between categories. It was notably high for predictions M and X, at 0.99 and 0.98, respectively. The GBC algorithm also demonstrated AUC values of 0.94 and 0.96 for predictions T and Z, indicating strong performance in managing more complex categories.

The precision in the M category was impressively high at 85.52%, demonstrating the model's ability to identify transition metals with few false positives. The X category also showed excellent precision at 90.18%, while 86.03% for Z reflects robust predictions but with slightly more misclassifications. Conversely, GBC exhibited a lower precision of 76.86% for T prediction, highlighting notable challenges with a higher likelihood of false positives.

Regarding the F1 score, which balances precision and recall, GBC achieved scores of 0.816 for M and 0.913 for X. T predictions yielded a lower F1 score of 0.744, indicating the necessity for additional fine-tuning. On a positive note, the GBC model attained an F1 score of 0.845 for Z, showcasing overall solid performance.

Finally, the computational efficiencies for each target prediction were assessed. The *TT* varied across all models, with the M prediction being the slowest at 1.071 s, while the X prediction was the fastest at 0.150 s. Predictions for T and Z were completed in 0.568 and 0.755 s, respectively, demonstrating that the GBC model maintained its efficiency despite handling complex datasets. However, predicting functional groups may require further improvement or additional data to enhance performance. Furthermore, the GBC algorithm possesses high AUC values, superior precision metrics, and short *TT*s, making it ideal for exploring varying component configurations forming different MXene structures.

To demonstrate this, we ultimately performed an inverse prediction of elemental descriptors corresponding to each category after assigning specific values for electrochemical features as inputs. The label-encoded data obtained as outputs were converted into their representative elemental descriptors and were used to construct the molecular formula of Z_k intercalated $M_{n+1}X_nT_x$ (n = 1) monolayer MXenes (**Table 3**).

By analyzing the feature importance plots of M, X, T, and Z categories (Figure S5, Supporting Information) and the predicted formulas in Table 3, we can correlate how varying electrochemical features (intercalation voltage, theoretical capacity, and in-plane lattice parameters) correspond to different monolayer MXene-based materials.

The theoretical capacity and in-plane lattice parameters (non-intercalated) are the most important features for predicting the M category, representing the transition element. MXenes with period IV (3d) transition metals like Sc, V, Ti, and Cr provide a greater gravimetric capacity compared to those made from heavier period V (4d) and VI (5d) transition metals such as Zr, Nb, Mo, Hf, and Ta.[28] Sc, characterized by its small ionic radius and light atomic mass, facilitates more effective ion accommodation and improves the charge storage capacity of the MXenes, suggesting favorable electrochemical properties.[28] In contrast, Zr is commonly incorporated into MXenes because of its chemical stability and larger atomic size. However, its high atomic mass generally leads to lower charge storage; hence, smaller gravimetric capacities. When we elevated the theoretical capacity from 400 to 500 mAh g^{-1}, the transition element in the Mg^{2+} intercalated

Table 3. The molecular formulas correspond to various ion-intercalated (i.e., Na^+, Li^+, Mg^{2+} MXene structures. These structures are predicted through single-target prediction using the GBC model. To achieve this, the user defines unseen data (not previously used for the AutoML training) for theoretical capacity, intercalation voltage, and in-plane lattice parameters for non-intercalated and intercalated MXenes. This information serves as input features for the inverse prediction of molecular descriptors.

Theoretical capacity [mAh g−1]	Intercalation voltage [V]	In-plane lattice parameter (non-intercalated) [Å]	In-plane lattice parameter (intercalated) [Å]	Molecular formula
200	1.0	3.75	3.92	$Li_2Sc_2CO_2$
300	0.5	3.085	3.42	Li_2Sc_2C
300	0.5	3.085	3.20	$Li_2Zr_2C(OH)_2$
300	1.0	3.085	3.20	$Na_2Zr_2CO_2$
300	1.0	3.12	3.31	Li_2Nb_2C
400	0.5	3.75	3.92	Mg_2Zr_2C
500	0.5	3.75	3.92	Mg_2Sc_2C
500	1.0	3.75	3.92	$Mg_2Sc_2CO_2$

MXenes changed from Zr to Sc, resulting in Sc_2C, which supports our earlier findings. Notably, while Sc is more advantageous for high-capacity energy storage systems, Zr-based MXenes are better suited for situations where structural stability is more critical.

For the center atom, X, the in-plane lattice parameter (non-intercalated) is the predominant feature affecting its prediction. In our predictions, C was favored in all categories over N, probably because carbides have larger lattice constants and longer bond lengths than nitrides, correlating with the atomic radii. Therefore, the assigned values for lattice parameters (3.085 to 3.92 Å) might be slightly in a higher range than those of N (typically smaller than 3.00 Å when intercalated), which did not allow N to be predicted as the center atom.[43]

Intercalation voltage is the most critical factor for T, or in other words, surface termination prediction.[28] All surface terminations affect how the material interacts with the surrounding ions, which alters the electrochemical behavior of the electrode. For instance, surface termination by —O promotes intercalation voltage and energy density increment, whereas —F terminations inhibit intercalation voltage but decrease capacity because of their large size, restricting ion mobility within the lattice. For instance, when Mg_2Sc_2C, Li_2Sc_2C, and Na_2Zr_2C are —O-terminated, the intercalation intercalation voltage raised from 0.5 to 1.0 V. —OH-terminated MXenes improve stability during charge-discharge cycles at a moderate intercalation voltage, as observed for the Li^+ intercalated Zr_2C scenario. Our results suggest that most MXene-based formulations showed higher intercalation voltage values when their surface is terminated with —O groups. As indicated earlier, a fraction of —OH groups may be converted into —O terminations by H_2O elimination upon drying of MXenes for high voltage battery development.[40]

Theoretical capacity is the most critical factor in predicting intercalating ions, denoted by category Z, which is, in turn, influenced by the surface termination. For instance, when the capacity was increased from 200 to 500 mAh g−1, the intercalating ion was shifted from Li^+ to Mg^{2+} for $Sc_2C(O)_2$ MXene. This result aligns with the previous simulations and experimental findings, which suggest that Mg^{2+} intercalation induces less lattice expansion but contributes to higher energy density due to its ability to store more charge per unit mass of the material.[43,44] Li-ions, on the other hand, strongly interact with MXenes via coulombic interactions,[40] and due to their small size, these materials demonstrate minimal lattice expansion upon intercalation comparable to that of Mg-ions. In this study, when the theoretical capacity was set to 300 mAh g−1 at 1 V intercalation voltage, Sc_2C MXene was intercalated with Li-ions; when this value increased to 500 mAh g^{-1}, the intercalation favored Mg-ions for the same MXene configuration. However, it is essential to mention that although Mg-ion batteries are one of the most promising candidates for energy storage, their slow diffusion in electrode materials can be the restrictive factor for long-term cycling performance; hence, the trade-off between high capacity and durability should be carefully considered before manufacturing.[45,46]

3. Conclusion and Future Perspectives

In this study, we demonstrated the capabilities of PyCaret's AutoML framework in predicting key electrochemical and structural properties of monolayer MXenes while performing inverse design to identify high-performing materials for energy storage applications. AutoML significantly reduces the time and expertise required to optimize material design by automating model selection, hyperparameter tuning, and performance evaluation. Among the regression models evaluated, CatBoost consistently outperformed, achieving high R^2 values across electrochemical and structural properties. Moreover, the framework's classification module enabled efficient inverse prediction, identifying promising Mg-intercalated MXenes (e.g., Sc_2CO_2) with high voltage and capacity metrics comparable to conventional materials like graphite and TiC_2. The proposed approach achieved similar prediction performance and accuracy yet more rapidly and with fewer codes than those that performed DFT calculations,[28] multi-target neural networks,[33] and conventional ML (Random Forest),[20] given in Table S3 (Supporting Information). This highlights the potential of AutoML-assisted frameworks to streamline structure-property investigations and accelerate material discovery. Notably, CatBoost's strength in managing categorical data stems from its intrinsic regressor characteristics. It employs ordered boosting across several decision trees, which helps the model avoid learning noise in the training data and reduces the risk of overfitting.[47,48] However, despite the strong performance reported here, relying solely on a single model while predicting may restrict the material discovery. Although CatBoost

handles categorical data and simplifies multi-categorical inputs, the added dimensionality can pose challenges. Future investigations should evaluate how well the model balances continuous variables with multi-categorical inputs to ensure nuanced information is preserved in the prediction process.

Inverse prediction-assisted material design gathers molecular formulas corresponding to different material structures based on predefined features. In the second part of our investigation, we performed an inverse prediction of MXenes using the classification module of PyCaret. First, we individually predicted each category (M, X, Z, T) using the classification module to determine the best-performing model. Gradient Boosting Classifier (GBC) was decided to be the best-performing model for all categories; therefore, it was used for molecular formulation prediction. Furthermore, PyCaret can provide a straightforward approach both for structure-property relationship predictions and for the inverse design of molecular formulas by efficiently navigating between high-dimensional design spaces without requiring extensive coding experience or manual model tuning. We found that Mg-intercalated MXenes both in pristine (non-functionalized) (Zr_2C, Sc_2C) and oxygen-terminated forms (Sc_2CO_2) are the ideal candidates for high-voltage/high-capacity energy storage applications, offering comparable performance to graphite and conventional TiC_2 MXenes (V > 0.5 V and a theoretical capacity > 400 mAh g−1), confirming the previous findings.[20,28,33] Although we are aware of the challenges in producing pristine MXenes, adapting alternative (post)synthesis and modification strategies could enable this, benefiting innovative MXene-based EES development.[49]

It is important to mention that our primary goal with this study is to introduce AutoML as a tool to support material science explorations, even with limited coding knowledge and resources. Consequently, the proposed study employed a training dataset of known MXene compositions. Future efforts should focus on expanding training datasets through computationally generated or experimental data to unlock new MXene configurations and properties. Potential examples include i) predicting properties of MXenes that are challenging to model using standard "direct" approaches, such as alloys with various "M" or "X" elements, (ii) identifying and clarifying an overlooked property, such as novel magnetic or optical traits, iii) discovering new analogs to MXenes (like MBenes),[50–52] iv) identifying novel terminal groups that confer properties distinct from the common O/OH/H/bare, such as recent studies on halogens,[53] or v) offering insights into improving synthesis yields and the long-term stability of MXenes.

Beyond MXenes, this methodology provides a flexible and accessible framework to investigate various material classes, including perovskites, alloys, and nanocomposites, with implications for energy storage and other functional material applications. By efficiently navigating high-dimensional design spaces, AutoML can unveil new compositions and optimize trade-offs among critical metrics such as capacity, charge/discharge rates, and stability. Future advancements in AutoML, such as multi-objective optimization and enhanced multi-target classification modules, will further refine material discovery pipelines, enabling the design of next-generation energy storage systems that effectively balance trade-offs among critical factors like capacity, charge/discharge rates, stability, and reproducibility. A significant limitation in employing data-driven approaches, like AutoML, that impedes unlocking their full potential is the absence of large, high-quality experimental datasets. One solution is integrating AutoML frameworks with hybrid models that merge theoretical simulations (e.g., DFT, MD simulations) and experimental feedback in a closed-loop system. This would facilitate real-time refinement of models and predictions, ensuring accuracy and applicability in practical settings. Such feedback-controlled workflows could bridge the gap between theory and experiment, offering a dynamic and iterative approach to material exploration.

In conclusion, AutoML represents a robust and accessible tool for accelerating material discovery and optimization. When combined with experimental validation, hybrid simulations, and multi-objective optimization, AutoML can unlock new opportunities in material design, potentially transforming the design and development of high-performance energy storage systems. The future of materials science lies in collaborative frameworks that blend data-driven approaches, theoretical insights, and experimental validation, ensuring impactful advancements across diverse application domains.

4. Experimental Section

Dataset Collection and AutoML Training: This study utilized a publicly available dataset generated via the Rashomon set[33] using the theoretical DFT-simulated data previously calculated to predict the electrochemical performance of different MXene-based electrode material configurations.[7] Briefly, the 360 different MXene-derivatives are represented with the formula of $M_{n+1}X_nT_xZ_k$, each varying based on the elemental compositions of the selected compound. The formula varies based on the type of center atom (X = C, N), the selection of transition elements (M = Sc, Ti, V, Cr, Zr, Nb, Mo, Hf, and Ta), either being functionalized or without functional groups (T = —H, —O, —OH, —F or NULL), intercalated (Z = Li^+, Na^+, K^+, and Mg^{2+}) or non-intercalated (NULL) with ions. The numerical data uniquely representing each MXene derivative molecular formula was converted into a machine-readable binary format (0 or 1) based on the presence or existence of specific components within a compound. The dataset contains 20 elements, meaning each compound is represented by a 20D binary vector (Sc, Ti, V, Cr, Zr, Nb, Mo, Hf, Ta, C, N, F, H, O, OH, NULL, Li, Na, K, and Mg). Additionally, these elemental descriptors, or 20D binary vectors (one-hot encoded categorical data), serve as input parameters to predict target features such as intercalation voltage, theoretical capacity, and in-plane lattice constants (ion intercalated and non-intercalated), thereby evaluating the predictive performance of each regression algorithm.

Google Colab environment utilizes an open-source low-code PyCaret framework (v.3.3.2) for AutoML model development and regressor analysis. Initially, the PyCaret environment was launched via the "*setup*" function, and a data transformation pipeline was created for subsequent data modeling and deployment. The dataset was divided into an 85/15% training/test split, and AutoML was performed. Subsequently, PyCaret took over the pre-processing, model training, and performance testing tasks, automatically trained 20 regression algorithms using DFT-simulated molecular descriptor data, and comparatively evaluated the models' performance in the target feature's prediction. To mitigate the effects of overfitting and ensure robust performance estimates, ten-fold cross-validation was performed on each training set to reduce overfitting. This technique involves partitioning the training data into ten subsets, training the model on nine subsets, and evaluating its performance on the held-out subset (Figure S1, Supporting Information). This process was repeated ten times, using a different subset for cross-validation each time, providing a more reliable assessment of the model's generalization capability. Hyperparameter tuning was achieved by automatically performing a random grid search.

Model Performance Evaluation: The performance of each model was evaluated using several metrics, including the coefficient of determination (R^2), mean absolute error (*MAE*), root mean squared error (*RMSE*), mean absolute percentage error (*MAPE*), and training time (*TT*). The R^2 metric measures the proportion of the predictable variance in the dependent variable based on the independent variables, indicating the model's explanatory power. *MAE* provides an average of the absolute errors between predicted and actual values, offering a simple measure of prediction accuracy. *RMSE* gives more weight to significant errors by taking the square root of the average of squared differences between prediction and actual observation, making it sensitive to outliers. *MAPE* provides a more straightforward way to measure and compare the prediction performance of ML models in target features by expressing errors as percentages. Its unitless nature allowed for the comparison of different physical quantities. However, MAPE became unstable or artificially low when the target variable was near zero, even with significant MAE. *TT* was a crucial factor in ML, referring to the time required for a selected model to process and learn from data. It was directly influenced by the model's complexity, the dataset size, and available computational resources. While faster *TT*s benefit scalability, real-time applications, and frequent re-training, a trade-off often exists between *TT* and model prediction performance. Therefore, optimizing *TT* without compromising performance was the key consideration when selecting a suitable model. Please refer to Table S1 (Supporting Information) document for more details regarding mathematical expressions for each performance metric evaluated in this study and their corresponding physical meaning.

Feature Importance Analyses: Feature importance analysis was a vital technique in ML for comprehending model behavior and data-generating processes.[50] To better grasp how the CatBoost model functions and the data it relies on, feature importance analyses were undertaken. This technique evaluated the relative impact of each feature on the model's predictive accuracy. Among the 20 regression algorithms created using Pycaret's AutoML capabilities, CatBoost emerged as the top-performing model based on its R^2 score. Consequently, global feature importance analyses were executed using the CatBoost model, with graphs illustrating the importance rankings of the elemental descriptors that influence the model's prediction performance for each target feature.

SHAP (SHapley Additive exPlanations) provided a comprehensive, game-theoretic perspective on how structural influences impact model predictions. SHAP analyses were performed to give a more detailed trajectory on feature importance and evaluate the contribution of individual elemental descriptors on the predicted intercalation voltage, theoretical capacity, and in-plane lattice constants. This reveals which features significantly affected each target property, allowing for deeper investigation and complementing global feature importance findings.

Inverse Prediction of Molecular Components: Predicting the molecular structures of electrode materials characterized by predetermined electrochemical properties (such as intercalation voltage and theoretical capacity) could greatly expedite material discovery, which was particularly beneficial in developing high-performance EES systems. Therefore, PyCaret's classification module was utilized to establish an inverse relationship between target features and input parameters. Briefly, the 20D dataset was condensed into a 4D vector that defined target features in four categories: M (transition metal), X (core atom), T (functional groups), and Z (intercalating ions). Then, the elemental descriptors (e.g., Sc, C) were label-encoded by converting categorical data into a machine-readable format (e.g., M: Sc → 0).

Following the labeling step, the experimental setup using AutoML's PyCaret classification module with the *setup() function* was established. The labeled dataset was divided into 85/15% splits for the classification algorithm's training and performance testing. To boost model reliability, we implemented ten-fold cross-validation (CV). 16 classification algorithms were assessed through PyCaret's *evaluate_model(sort = "accuracy")* function, computing performance metrics like accuracy, area under the curve (AUC), recall, precision, F1-score, and *TT*, and sorting them based on model AUC values. The model with the highest AUC value was chosen for further assessment using the *evaluate_models()* function, which provided insights through the confusion matrix, receiver operating characteristic (ROC) curve, and global feature of importance analyses.

After determining GBC as the best-performing model for each category's prediction, it was utilized for the inverse prediction of single categories (M, X, Z, T) constituting molecular formulas. All hyperparameters used to develop regression and classification algorithms are listed in the *Supporting Information* document (Table S4, Supporting Information). For the prediction of molecular compounds, numerical values were randomly assigned to each electrochemical property as an input: intercalation voltage was varied between 0.5 and 1.0 V, theoretical capacity from 200 to 500 mAh g^{-1}, and in-plane lattice constants ranging from 2.90 to 3.92 Å, according to the previous literature.[20,28,33] An example workflow is given as follows. First, the inputs for intercalation voltage, capacity, and in-plane lattice constants (intercalated versus non-intercalated) were set at 0.50 V, 300 mAh g^{-1}, 3.92, and 3.085 Å, respectively. Next, each molecular component was predicted by merging the categorical outputs in the general formula of monolayer MXenes: $Z_kX_{n+1}C_nT_x$ →. [4, 0, 3, 0] The predicted molecular formula is ultimately formed as $Li_2Zr_2C(OH)_2$.

Supporting Information

Supporting Information is available from the Wiley Online Library or from the author.

Acknowledgements

B.A. and G.K. contributed equally to this work. The illustrative figures were created with Biorender.com.

Conflict of Interest

The authors declare no conflict of interest.

Data Availability Statement

The data that support the findings of this study are available from the corresponding author upon reasonable request.

Keywords

feature importance, intercalation voltage, molecular formula prediction, PyCaret, theoretical capacity

Received: October 27, 2024
Revised: February 14, 2025
Published online:

[1] A. Manthiram, *MRS Bull.* **2016**, *41*, 624.
[2] P. G. Nikhil, G. Sivaramakrishnan, Electro-Chemical Battery Energy Storage Systems-A Comprehensive Overview. Energy Storage **2011**, 229, https://doi.org/10.1002/9781119555599.ch7.
[3] S. Isah, *Asian J. Nano. Mat.* **2018**, *1*, 90.
[4] M. Naguib, M. Kurtoglu, V. Presser, J. Lu, J. Niu, M. Heon, L. Hultman, Y. Gogotsi, M. W. Barsoum, *Adv. Mater.* **2011**, *23*, 4248.
[5] H. An, T. Habib, S. Shah, H. Gao, M. Radovic, M. J. Green, J. L. Lutkenhaus, *Sci. Adv.* **2018**, *4*, eaaq0118.
[6] M. Naguib, V. N. Mochalin, M. W. Barsoum, Y. Gogotsi, *Adv. Mater.* **2014**, *26*, 992.

[7] C. Eames, M. S. Islam, *J. Am. Chem. Soc.* **2014**, *136*, 16270.
[8] J. Luo, W. Zhang, H. Yuan, C. Jin, L. Zhang, H. Huang, C. Liang, Y. Xia, J. Zhang, Y. Gan, X. Tao, *ACS Nano* **2017**, *11*, 2459.
[9] X. Li, Z. Huang, C. E. Shuck, G. Liang, Y. Gogotsi, C. Zhi, *Nat. Rev. Chem.* **2022**, *6*, 389.
[10] J. Pang, R. G. Mendes, A. Bachmatiuk, L. Zhao, H. Q. Ta, T. Gemming, H. Liu, Z. Liu, M. H. Rummeli, *Chem. Soc. Rev.* **2019**, *48*, 72.
[11] Y. Gogotsi, *MXenes: From Discovery to Applications of Two-Dimensional Metal Carbides and Nitrides*, CRC Press, Boca Raton, FL, USA **2023**.
[12] P. K. Panda, D. Singh, R. Ahuja, *Next-Generation Materials for Batteries*, AIP Publishing, New York **2021**, 1.
[13] Q. He, B. Yu, Z. Li, Y. Zhao, *Energy Environ. Mater.* **2019**, *2*, 264.
[14] A. Van Der Ven, Z. Deng, S. Banerjee, S. P. Ong, *Chem. Rev.* **2020**, *120*, 6977.
[15] D. Atkins, E. Ayerbe, A. Benayad, F. G. Capone, M. R. Johnson, H. Li, J. Maria, G. Lastra, M. L. D. Souza, V. Meunier, M. Morcrette, H. Reichert, P. Simon, J.-P. Rueff, J. Sottmann, W. Wenzel, A. Grimaud, **2021**, *12*, 2102687.
[16] J. Orangi, M. Beidaghi, *Adv. Funct. Mater.* **2020**, *30*, 2005305.
[17] P. Domingos, *Commun. ACM* **2012**, *55*, 78.
[18] V. L. Deringer, *J. Physics: Energy* **2020**, *2*, 041003.
[19] E. Asadi Shamsabadi, N. Roshan, S. A. Hadigheh, M. L. Nehdi, A. Khodabakhshian, M. Ghalehnovi, *Constr. Build. Mater.* **2022**, *324*, 126592.
[20] S. Li, A. S. Barnard, *Chem. Mater.* **2022**, *34*, 4964.
[21] S. S. Pakzad, N. Roshan, M. Ghalehnovi, *Sci. Rep.* **2023**, *13*, 3646.
[22] A. Metin, T. T. Bilgin, *Peer J. Comput. Sci.* **2024**, *10*, e2188.
[23] S. K. K. Santu, M. D. Hassan, M. J. Smith, L. Xu, C. Zhai, K. Veeramachaneni, *ACM Comput. Surv.* **2020**, *54*, 1.
[24] P. Gijsbers, E. LeDell, J. Thomas, S. Poirier, B. Bischl, J. Vanschoren, *arXiv* **2019**.
[25] H. Eldeeb, M. Maher, R. Elshawi, S. Sakr, *Expert Syst Appl.* **2024**, *243*, 122877.
[26] GitHub – pycaret/pycaret: An open-source, low-code machine learning library in Python, https://github.com/pycaret/pycaret (Accessed: October 2024).
[27] O. Topsakal, T. C. Akinci, *Balkan J. Electr. Comput. Eng.* **2023**, *11*, 257.
[28] C. Eames, M. S. Islam, *J. Am. Chem. Soc.* **2014**, *136*, 16270.
[29] A. Vehtari, A. Gelman, J. Gabry, *Stat. Comput.* **2017**, *27*, 1413.
[30] G. Cherkashinin, R. Hausbrand, W. Jaegermann, *J. Electrochem. Soc.* **2019**, *166*, A5308.
[31] M. Sen, M. Ozcan, Y. R. Eker, *Next Sustainability* **2024**, *3*, 100036.
[32] A. Eftekhari, *ACS Sustain. Chem. Eng.* **2019**, *7*, 3684.
[33] S. Li, A. S. Barnard, *Cell Rep. Phys. Sci.* **2023**, *4*, 101675.
[34] J. Betz, G. Bieker, P. Meister, T. Placke, M. Winter, R. Schmuch, *Adv. Energy Mater.* **2019**, *9*, 1803170.
[35] M. D. Radin, S. Hy, M. Sina, C. Fang, H. Liu, J. Vinckeviciute, M. Zhang, M. S. Whittingham, Y. S. Meng, A. Van der Ven, *Adv. Energy Mater.* **2017**, *7*, 1602888.
[36] A. Y. S. Eng, C. B. Soni, Y. Lum, E. Khoo, Z. Yao, S. K. Vineeth, V. Kumar, J. Lu, C. S. Johnson, C. Wolverton, Z. W. Seh, *Sci. Adv.* **2022**, *8*, 2422.
[37] D. Er, J. Li, M. Naguib, Y. Gogotsi, V. B. Shenoy, *ACS Appl. Mater. Interfaces* **2014**, *6*, 11173.
[38] M. Ghidiu, M. R. Lukatskaya, M. Q. Zhao, Y. Gogotsi, M. W. Barsoum, *Nature* **2014**, *516*, 78.
[39] B. Anasori, M. R. Lukatskaya, Y. Gogotsi, *Nat. Mater.* **2017**, *2*, 1.
[40] M. Naguib, V. N. Mochalin, M. W. Barsoum, Y. Gogotsi, *Adv. Mater.* **2014**, *26*, 992.
[41] J. Li, M. Lu, W. Zheng, W. Zhang, *Energy Storage Mater.* **2024**, *64*, 103068.
[42] J. Zhou, X. Zha, F. Y. Chen, Q. Ye, P. Eklund, S. Du, Q. Huang, *Angew. Chem., Int. Ed.* **2016**, *55*, 5008.
[43] Y. Xie, P. R. C. Kent, *Phys. Rev. B Condens. Matter Mater. Phys.* **2013**, *87*, 235441.
[44] Z. Zhao-Karger, M. Fichtner, *Front. Chem.* **2018**, *6*, 00656.
[45] B. Raisi, X. Liu, J. Rahmatinejad, Z. Ye, *Small Methods* **2024**, *8*, 2400004.
[46] M. R. Lukatskaya, O. Mashtalir, C. E. Ren, Y. Dall'agnese, P. Rozier, P.-L. Taberna, M. Naguib, P. Simon, M. W. Barsoum, Y. Gogotsi, *Science* **2013**, *341*, 1502.
[47] A. V. Dorogush, V. Ershov, A. G. Yandex, "CatBoost: gradient boosting with categorical 840 features support" https://arxiv.org/abs/1810.11363v1 (Accessed: October 2024).
[48] L. Prokhorenkova, G. Gusev, A. Vorobev, A. V. Dorogush, A. Gulin **2017**, https://doi.org/10.48550/arXiv.1706.09516.
[49] U. Yorulmaz, I. Demiroglu, D. Çakir, O. Gülseren, C. Sevik, *J. Phys.: Energy* **2020**, *2*, 032006.
[50] A. Hayat, T. Bashir, A. M. Ahmed, Z. Ajmal, M. M. Alghamdi, A. A. El-Zahhar, M. Sohail, M. A. Amin, Y. Al-Hadeethi, E. Ghasali, S. Raza, Y. Orooji, *Mater. Sci. Eng. R: Rep.* **2024**, *159*, 100796.
[51] M. S. Javed, X. Zhang, T. Ahmad, M. Usman, S. S. A. Shah, A. Ahmad, I. Hussain, S. Majeed, M. R. Khawar, D. Choi, C. Xia, W. Al Zoubi, M. A. Assiri, A. M. Hassan, S. Ali, W. Han, *Mater. Today* **2024**, *74*, 121.
[52] J. Chen, W. Zhang, R. Chen, Y. Dai, J. Zhang, H. Yang, W. Zong, Z. Jiang, Y. Zhong, J. Wang, X. Zhang, G. He, *Adv. Energy Mater.* **2024**, https://doi.org/10.1002/aenm.202403757.
[53] M. Dahlqvist, J. Rosen, *npj 2D Mater. Appl.* **2024**, *8*, 65.